

SP84-MSFC-2726

SP84-MSFC-2726

N84-25584

Final Report

RESEARCH IN SOLAR PHYSICS:  
SOME TECHNIQUES FOR ANALYZING DATA  
FROM THE ULTRAVIOLET SPECTROMETER  
AND POLARIMETER

April 1984



**TELEDYNE  
BROWN ENGINEERING**

Cummings Research Park • Huntsville, Alabama 35807



FINAL REPORT  
SP84-MSFC-2726

RESEARCH IN SOLAR PHYSICS:  
SOME TECHNIQUES FOR ANALYZING DATA FROM THE  
ULTRAVIOLET SPECTROMETER AND POLARIMETER

By  
William Henze Jr.

April 1984

Prepared For  
SPACE SCIENCE LABORATORY  
GEORGE C. MARSHALL SPACE FLIGHT CENTER  
MARSHALL SPACE FLIGHT CENTER, ALABAMA 35812

Contract No. NAS8-31908

Prepared By  
SPACE SYSTEMS DEPARTMENT  
SPACE PROGRAMS DIVISION  
TELEDYNE BROWN ENGINEERING  
HUNTSVILLE, AL 35807

## ACKNOWLEDGEMENTS

Much of the scientific effort performed under this contract was done in collaboration with colleagues, primarily at the Marshall Space Flight Center, Goddard Space Flight Center, Lockheed Palo Alto Research Laboratory, and High Altitude Observatory.

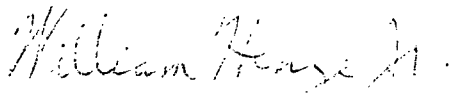
The basic structure and some of the components of the UVSP instrument were taken from the engineering model (the flight spare) of the ultraviolet spectrometer flown on OSO-8. The original OSO-8 instrument was built by the Laboratory of Atmospheric and Space Physics of the University of Colorado. Most of the modifications to the OSO-8 hardware and the integration of the instrument were performed by the General Electric Company, Valley Forge, Pennsylvania, with overall systems design and engineering by the Goddard Space Flight Center. The optical design and optical parts fabrication were also provided by the Goddard Space Flight Center. The polarimeter was designed and built by the Marshall Space Flight Center. The electronics, including the instrument computer, were built by SCI Systems, Huntsville, Alabama. Software for the instrument computer was provided by the Lockheed Palo Alto Research Laboratory, Palo Alto, California. Command generation software for the ground computer at Goddard was also supplied by Lockheed while most of the data reduction software was provided by the Goddard Space Flight Center.

## ABSTRACT

This report contains useful information for certain aspects of the analysis of data obtained by the Ultraviolet Spectrometer and Polarimeter (UVSP) on the Solar Maximum Mission (SMM). The first section describes the meaning of the UVSP co-ordinate system and the SMM roll, pitch, and yaw and then explains how to overlay UVSP images. The second section contains a description of various computer programs that calculate the line-of-sight component of the SMM spacecraft velocity from the spacecraft to the Sun. The spacecraft velocity can be used to correct or interpret the signal observed in UVSP dopplergrams. This is applied in the third section which describes a method of using the spacecraft velocity to calibrate UVSP dopplergrams and magnetograms, i.e., determine the width of the observed emission line. The fourth section describes UVSP polarization analysis procedures while the fifth section gives expressions for the statistical uncertainties in various quantities obtained from UVSP measurements.

Note that the equation numbers in each section begin again at Equation (1).

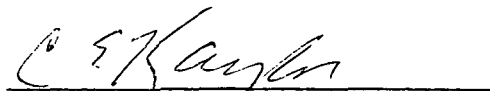
Submitted by:



---

William Henze Jr.  
Principal Investigator

Approved by:



---

C. E. Kaylor  
Project Manager

## TABLE OF CONTENTS

	Page
Chapter 1	1
1.1	1
1.2	1
1.3	4
1.4	5
1.5	5
1.6	6
1.7	7
1.8	7
Chapter 2	8
2.1	8
2.2	9
2.3	9
2.4	9
2.5	10
2.6	11
2.7	11
Chapter 3	14
3.1	14
3.2	15
3.3	17
3.4	18
3.5	23
3.6	23

TABLE OF CONTENTS  
(Concl.)

	Page
Chapter 4 UVSP Polarization Analysis Procedures . . . . .	24
4.1 Polarization Signal . . . . .	24
4.2 Magnetograms . . . . .	25
4.3 Polargrams . . . . .	25
Chapter 5 Statistical Uncertainties . . . . .	27
5.1 Background . . . . .	27
5.2 Polarization . . . . .	28
5.3 Line Intensities . . . . .	29
5.4 Magnetometry . . . . .	29
5.5 Velocity Measurements . . . . .	30
References . . . . .	32

## LIST OF ILLUSTRATIONS

Figure	Title	Page
1-1	Orientation of SMM and UVSP Coordinate Systems . . . . .	2
1-2	Definition and Scale of UVSP Coordinate System and Field of View . . . . .	2
1-3	Example of Typical Observation . . . . .	3
3-1	Example Illustrating the method described in this paper. Data are for Pixel 5 in UVSP Experiment 14398 obtained 25 October 1980, 00:33 - 00:54 UT . . . . .	19

## LIST OF TABLES

Table	Title	Page
I	Offset Velocity, Doppler Width, and Longitudinal Magnetic Field, UVSP Experiment 14398 . . . . .	21
II	Comparison of Methods of Calibration of the Line Width, UVSP Experiment 14302 . . . . .	22



# CHAPTER 1

## ORIENTING AND OVERLAYING UVSP IMAGES

### 1.1 PURPOSE

The purpose of this chapter is to provide to users of the UVSP data explanations of the orientation and coordinate systems applicable to UVSP images and of how to overlay different UVSP images and determine their position relative to the sun. The UVSP instrument and overall experiment have been described by Woodgate et al. (1980) and Henze (1979).

### 1.2 DEFINITIONS OF COORDINATES AND PARAMETERS

The orientation of the SMM and UVSP coordinate systems is shown in Figure 1-1. The definition of the UVSP coordinate system is illustrated in Figure 1-2. An example of a typical observation showing the signs of the various coordinates is given in Figure 1-3 which also shows the definition of the angle theta used in the UVSP Data Catalog.

The pitch and yaw angles and the UVSP X and Y coordinates are given in arcseconds. The roll and theta angles are given in degrees.

- SMM Roll Angle - positive when spacecraft is rolled from solar north toward west, i.e., clockwise
- SMM Pitch Angle - positive when spacecraft is pointed south of sun center when roll angle is zero
- SMM Yaw Angle - positive when spacecraft is pointed east of sun center when roll angle is zero
- UVSP X Coordinate - positive toward north when roll angle is zero
- UVSP Y Coordinate - positive toward east when roll angle is zero
- Theta Angle in UVSP Data Catalog - positive from north toward east, i.e., counterclockwise.

The pitch and yaw angles are measured from the center of the solar disk and refer to an arbitrary spacecraft "boresight", the definition of which was changed to least twice during the mission. It was, however, always located within the lower left quadrant of the UVSP field of view. It is possible that up until July 1980 there may have been a center-to-limb difference in the location of the spacecraft "boresight". For periods of up to one or two days, it is likely that the "boresight" position did

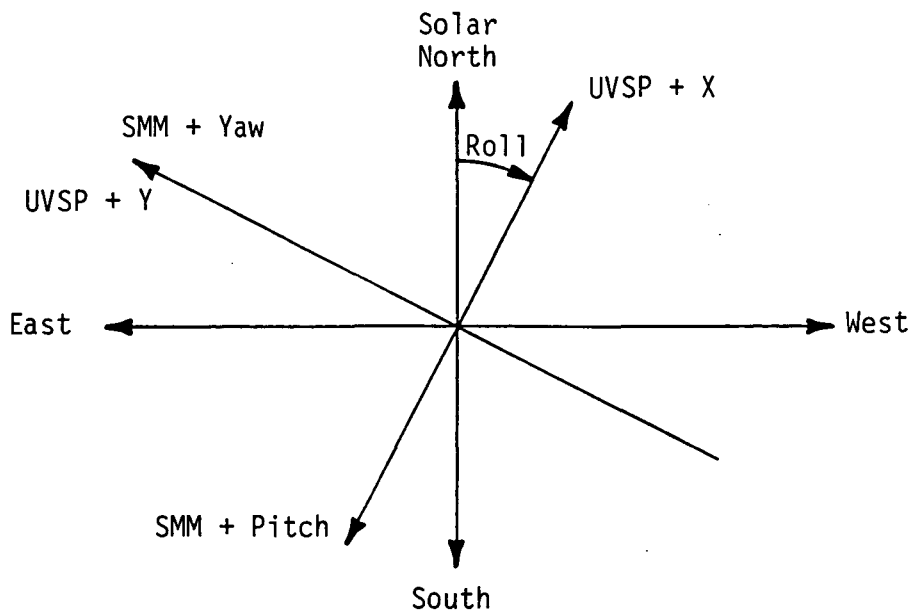


Figure 1-1. Orientation of SMM and UVSP Coordinate Systems

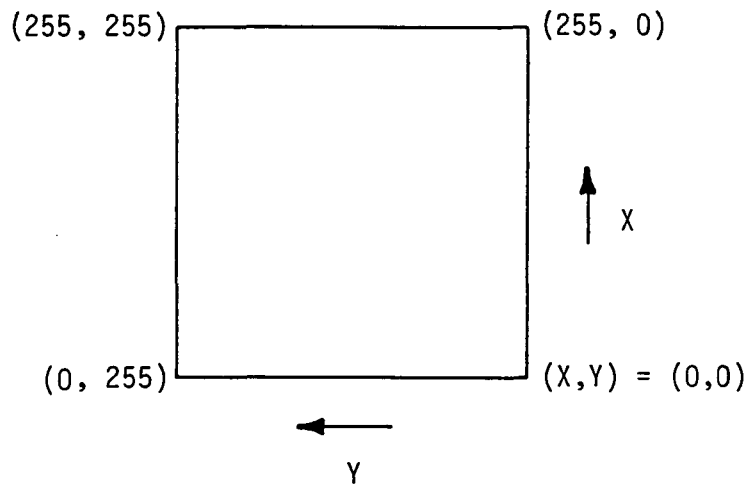


FIGURE 1-2. Definition and Scale of UVSP Coordinate System and Field of View. X and Y are always given in integer arcseconds.

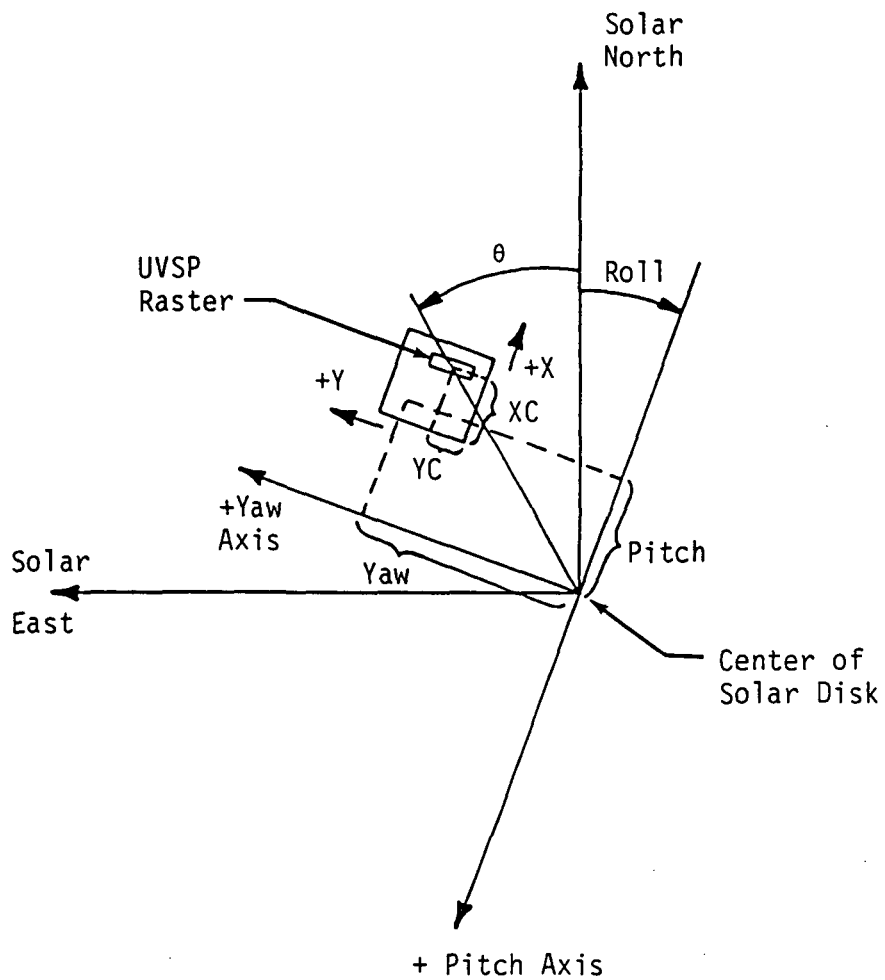


Figure 1-3. Example of Typical Observation. For this example, Pitch is negative and Yaw, Roll, and Theta ( $\theta$ ) are positive. Of course, X and Y are always either zero or positive.

not change more than a few arcsec which is the probable accuracy of the whole SMM pointing scheme.

The UVSP coordinate system shown in Figure 1-2 is a 256 x 256 arcsec array of possible UVSP pointing positions or pixel centers. Because many of the entrance slits are larger than 1 arcsec square, the actual possible UVSP field-of-view is larger than 256 arcsec square.

Further quantities associated with a given UVSP data set or experiment number are the following:

XCEN or XC = X coordinate associated with the center of a UVSP raster.

YCEN or YC = Y coordinate associated with the center of a UVSP raster.

NX = number of X positions in a UVSP raster  
= number of pixels in X direction.

NY = number of Y positions in a UVSP raster  
= number of pixels in Y direction.

DX = spacing in arcsec between centers of adjacent pixels in X direction.

DY = spacing in arcsec between centers of adjacent pixels in Y direction.

Note that DX and DY are not necessarily the same as the corresponding dimensions of the entrance slit, although they are usually chosen to be the same.

### 1.3 DATA OBSERVING AND STORAGE ORDER

In the raster, the value of X or Y corresponding to the outer loop would be set at its minimum value for that raster and observations would be taken while the value of X or Y corresponding to the inner loop would step from its minimum to its maximum value. The outer loop would then step to its next higher value and the inner loop would again step from minimum to maximum value. The usual nesting of loops had X as the inner loop and Y as the outer loop. This meant that the data were taken in vertical strips beginning at the lower right. In other words, the very first data point which is the same as the first point of the first strip was located at the lower right corner of the raster. The last point of the first strip was located at the upper right corner. The first point of the last strip was located at the lower left corner. The last point of the last strip which is the same as the very last data point of the whole raster was located at

the upper left corner. In the usual situation where the SMM roll angle was zero, north was up and east was to the left. Many display programs orient the rasters properly (i.e., the rasters are flipped in the computer).

#### 1.4 MEANING OF RASTER CENTER COORDINATES

XCEN and YCEN are stored in Junior's DMA and also in the experiment header block of the reformatted data files. The positioning of the raster can depend on whether NX, NY, DX, DY are odd or even. The explanation given below applies to the X parameters. An identical but separate explanation applies to the Y parameters.

NX Odd: If NX is odd, then the central strip of pixels, i.e., the  $[(NX+1)/2]^{\text{th}}$  strip counting in the X direction, is centered exactly at XCEN.

NX Even and DX Even: The boundary between the two central strips of pixels, i.e., the  $(NX/2)^{\text{th}}$  and  $[(NX/2)+1]^{\text{th}}$  strips counting in the X direction, is located exactly at XCEN. The coordinates of the two strips are  $XCEN \pm DX/2$ .

NX Even and DX Odd: Because the spacing DX is an odd number of arcseconds, the real center of the raster - the boundary between the two central strips of pixels, i.e., the  $(NX/2)^{\text{th}}$  and  $[(NX/2)+1]^{\text{th}}$  strips counting in the X direction - is not actually at an integer X coordinate value. The boundary between the two central strips is located at  $XCEN + \frac{1}{2}$ . Thus, the X coordinates for the two central strips counting in the X direction are  $XCEN - [(DX-1)/2]$  and  $XCEN + [(DX+1)/2]$ .

#### 1.5 LOCATION OF EDGE PIXELS IN UVSP COORDINATES

Because contour plots treat the pixels as points rather than squares or rectangles, it is necessary to find the location of the center of the edge pixels, i.e., the pointing coordinates for the edge pixels. This means that the spread in the coordinates for the edge pixels at opposite sides of the raster is not the same as the field of view because the field of view includes the size of the entrance slit.

X Coordinate for Edge Pixels

	Upper	Lower
NX Odd	$XCEN + \frac{(NX-1)}{2} * DX$	$XCEN - \frac{(NX-1)}{2} * DX$
NX Even, DX Even	$XCEN + (NX-1) * \frac{DX}{2}$	$XCEN - (NX-1) * \frac{DX}{2}$
NX Even, DX Odd	$XCEN - \frac{(DX-1)}{2} + \left(\frac{NX}{2} * DX\right)$ or $XCEN + \frac{1}{2} [(NX-1)*DX+1]$	$XCEN + \frac{(DX+1)}{2} - \left(\frac{NX}{2} * DX\right)$ or $XCEN - \frac{(DX-1)}{2} - \left(\frac{NX}{2} - 1\right) * DX$ or $XCEN - \frac{1}{2} [(NX-1) * DX - 1]$

Again, a similar set of expressions involving NY and DY is applicable for the Y coordinate of the left and right edge pixels.

1.6 OVERLAYING RASTERS IN UVSP COORDINATES

When feature tracking was being used and the rasters were not too far separated in time, one can simply determine the X and Y coordinates of the upper left corner pixel in each raster, subtract the underlay coordinates from the overlay coordinates to find the position of the upper left pixel of the overlay relative to the upper left corner of the underlay, and then place the overlay on the underlay using the position in arcsec of the upper left corner of the overlay relative to the upper left corner of the underlay. Of course, the scales of both rasters should be the same. To determine the scale, one should recall that the number of arcsec between the pixel centers on the top edge and on the bottom edge is  $(NX-1)*DX$ ; a similar expression applies in the Y direction. On the other hand, some contour plots are surrounded by a box that corresponds to dimensions of  $NX*DX$  and  $NY*DY$ ; in such plots the contour lines do not fill up the entire box, i.e., there are blank strips one pixel wide along the adjacent edges.

## 1.7 OVERLAYING RASTERS IN PIXEL NUMBERS

Because contour plots are sometimes labelled in pixel numbers, it is then convenient to use the underlay pixel number scale as the coordinate system. One goes through the process described in Section 1.6 above and then divides the offsets by the underlay values of DX and DY. If the pixel number scale has its origin at the upper left and if the contour plots are pushed into the upper left corner (i.e., if the blank strips are at the bottom and right edges), then the upper left corner of the overlay can be positioned directly on the underlay using the underlay pixel number scale. (Of course, the upper left corner of the overlay could be outside the box on the underlay.)

## 1.8 CORRECTING FOR SOLAR ROTATION: SPACECRAFT PITCH AND YAW

If feature tracking was not being used, it is necessary to correct for solar rotation. One should calculate the number of arcsec by which a feature would have shifted to the west (usually to the right) in the later raster. If the pitch and yaw were unchanged, then one would simply shift the later raster to the east (usually left) by the appropriate number of arcsec caused by rotation. If the pitch and yaw were changed, then one should also shift one of the rasters in the proper direction.

CHAPTER 2  
SPACECRAFT VELOCITY PROGRAMS - COMPONENT  
OF ORBITAL VELOCITY ALONG LINE OF SIGHT TO SUN

2.1 INTRODUCTION

This chapter describes Fortran and IDL programs and subprograms and associated data files which are utilized to calculate the component of the orbital spacecraft velocity along the line of sight to the sun at any time during the useful part of the SMM mission in 1980.

Definitions for some of the symbols are as follows:

VLOS = Line-of-sight component of velocity relative to sun in  $\text{km s}^{-1}$ . Negative when spacecraft is moving toward the sun, i.e., before orbital noon; positive when moving away from the sun, i.e., after orbital noon. Floating point.

IDOY = Day of year for which velocity is desired. Integer.

FRD = Time expressed as fraction of day for which velocity is desired. Floating point.

IOPEN = Code in some versions of the IDL procedures. It indicates whether the call is the first one ( $IOPEN = 0$ ) or a second or following call ( $IOPEN \neq 0$ ). During the first call to VELSCI, IOPEN is set equal to a non-zero number so that if the calling program or procedure uses a variable instead of a constant for that parameter, then the same variable can be used in following calls without changing its value; it must have been set equal to zero before the first call. Integer.

Someone who wants to use the Fortran subroutines and IDL procedures without learning any background can read Sections 2.2 and 2.3 only. The explanation of the method is given in Section 2.4. Section 2.5 describes the programs used to create the data files containing the tables of orbital information required; Section 2.6 describes the data files themselves. Section 2.7 describes the different versions of the Fortran subroutines and the IDL procedures available for the calculation of the line-of-sight velocity relative to the sun.



## 2.2 FASTER AVAILABLE VERSIONS OF THE VELOCITY CALCULATION SUBPROGRAMS FOR INDIVIDUAL TIMES - SHORT LISTING

The subprograms listed here open and read in the data file on the first call only. The second and following calls should be much faster. For explanation, see the later sections.

### 2.2.1 Fortran

VELSC2.FTN - contains SUBROUTINE VELSC(IDOY,FRD,VLOS).  
This version of VELSC uses data file BETAT1.DAT.

### 2.2.2 IDL

It is not known which of the versions in the two files given here is faster. All parameters must be scalars.

VELSC2.PRO - contains PRO VELSCI,IDOY,FRD,VLOS,IOPEN.  
This version of VELSCI uses data file BETAT1.DAT.

VELSC4.PRO - contains PRO VELSCI,IDOY,FRD,VLOS,IOPEN.  
This version of VELSCI uses data file BETAT3.DAT.

## 2.3 IDL VELOCITY CALCULATION PROCEDURES TO HANDLE ONE-DIMENSIONAL ARRAYS FOR INPUT PARAMETERS - SHORT LISTING

It is not known which of the versions given here is faster. The time FRD (in fraction-of-day units) and the velocity VLOS can be one-dimensional arrays (same size); the times in FRD should be all in the same orbit. VLOS is always a scalar.

VELSC1.PRO - contains PRO VELSC,IDOY,FRD,VLOS. This version of VELSC uses data file BETAT1.DAT.

VELSC3.PRO - contains PRO VELSC,IDOY,FRD,VLOS. This version of VELSC uses data file BETAT3.DAT.

## 2.4 METHOD

It is assumed that the spacecraft orbit is circular and that the orbit of the earth is circular. We thus ignore any motion of the earth toward or away from the sun. At the present time, the circular spacecraft velocity is assumed to be constant over the entire mission.

The equation for the component of the spacecraft velocity along the line of sight to the sun,  $V_{||}$ , is

$$V_{||} = V_0 \sin \left[ 2\pi \left( \frac{t-t_0}{T} \right) \right] \cos \beta$$

where  $t_0$  = time of spacecraft noon for this orbit,  
 $t$  = time for which  $V_{||}$  is being calculated,  
 $T$  = orbital period of spacecraft,  
 $V_0$  = spacecraft orbital velocity,  
 $\beta$  = angle between spacecraft orbital plane and direction toward sun.

The time of spacecraft noon is interpolated from a table with entries usually spaced every 7 to 10 orbits. The value of  $\beta$  is also interpolated from the same table. The table is based on the orbital predictions contained in the blue books in the EOF at GSFC. The relevant information is on the right hand side of the pages of the Equator Crossing List which usually appears in both Volumes I and II of the blue books. Orbital noon is the same as the time of maximum solar elevation.

## 2.5 PROGRAMS TO GENERATE DATA TABLES

### VSCDAT1.FTN,.TSK

Fortran program to create and/or add to file BETAT1.DAT; inserts new data from keyboard into proper location in table in file. Old version of file BETAT1.DAT should be purged after new data have been inserted. The FTN file contains the statement INCLUDE DOY.FTN.

### DOY.FTN

Fortran SUBROUTINE DOY(IDOY,IYR,IMON,IDOM). Calculates day-of-year for input year, month, day-of-month. Used by VSCDAT1 because blue book with times of orbital noon and  $\beta$  gives month and day-of-month instead of day-of-year.

### VSCDAT3.PRO.

IDL program which creates file BETAT3.DAT based on input file BETAT1.DAT to allow IDL ASSOC function to be used for reading in data table. This program should be run every time file BETAT1.DAT is changed and the old version of BETAT3.DAT should be deleted before running VSCDAT3.PRO or purged afterward.

## 2.6 FILES CONTAINING DATA TABLES

### BETAT1.DAT

ASCII data table containing  $\beta$  angle and time of orbital noon for whichever orbits were entered. For 1980 only. Order of entries is according to time. Each record contains  $\beta$  (in degrees), day-of-year, hr, min, sec with format (F10.3, 4I7). Can be printed out with PIP. At the present time, the spacing between entries is usually 7 to 10 orbits; however, additional orbits can always be inserted using VSCDAT1. An editor can also be used to insert additional entries or delete mistakes; however, care must be taken to insert the new entry into the proper position according to the time.

### BETAT3.DAT

Data table created by IDL program VSCDAT3.PRO and containing primarily  $\beta$  angle and time of orbital noon for whichever orbits were in BETAT1.DAT. Each record contains three unformatted (binary) floating point numbers. Each number in the first record (IDL record 0) is equal to the number of entries of  $\beta$  and time in the table. Let the number of entries be NSIZ. Then the total number of records in BETAT3.DAT = NSIZ + 1 which is one greater than the number of records in BETAT1.DAT. For the second and following records in BETAT3.DAT (IDL records 1 through NSIZ), the first number is  $\beta$  in degrees, the second number is the day-of-year (remember, in floating point), and the third number is the time in fraction-of-a-day. The reason for storing the DOY and fraction-of-day separately is to preserve significant figures. This file can be read with the IDL ASSOC function.

## 2.7 SUBPROGRAMS WHICH CALCULATE THE LINE-OF-SIGHT COMPONENT OF SPACECRAFT VELOCITY RELATIVE TO THE SUN

The Fortran subroutines and IDL procedures all calculate the line-of-sight velocity component VLOS (in  $\text{km s}^{-1}$ ) for a given day-of-year IDOY and fractional time-of-day FRD in 1980.

### 2.7.1 Fortran Subroutines

Both files contain a SUBROUTINE VELSC(IDOY,FRD,VLOS).

Both subroutines use data file BETAT1.DAT.

#### VELSC1.FTN

For each call to VELSC, opens file BETAT1.DAT and reads individual records until the required records are found. Slow.

#### VELSC2.FTN

On first call only to VELSC, opens and reads in entire file BETAT1.DAT which is then saved in memory. Search through table on following calls (and also on first call) is made by searching through table already stored in memory. Faster for second and following calls.

### 2.7.2 IDL Procedures

The files contain either PRO VELSC, IDOY, FRD, VLOS or PRO VELSCI, IDOY, FRD, VLOS, IOPEN which do same thing as Fortran Subroutine described above. Procedure VELSCI includes the parameter IOPEN to indicate whether the call is the first one (IOPEN = 0) or a second or following call (IOPEN  $\neq$  0); on the first call, the data file is opened and read in its entirety, and the resulting table is saved in COMMON BLOCK so that it does not need to be read in again on following calls. The parameter IOPEN is set equal to a non-zero number in the procedure VELSCI during the first call so that if the calling program or procedure uses a variable for that parameter instead of a constant, then the same variable can be used in the following calls without changing its value; of course it must be set equal to zero before the first call. Procedure VELSC opens data file and reads individual records for each call and should therefore be slower than VELSCI for the second and following calls for individual times. However VELSC can handle one-dimensional arrays (same size) for FRD and VLOS; the times in FRD should be in the same orbit. The velocity is calculated using IDL array arithmetic which should be faster for arrays. IDOY is always a scalar.

VELSC1.PRO - contains VELSC (IDL procedure). Uses BETAT1.DAT. Slow for individual times but can handle one-dimensional arrays for FRD and VLSO.

VELSC2.PRO - contains VELSCI (IDL procedure). Uses BETAT1.DAT. Faster for second and following calls. FRD and VLOS are scalar.

VELSC3.PRO - contains VELSC (IDL procedure). Uses BETAT3.DAT. Slow for individual times but can handle one-dimensional arrays for FRD and VLOS.

VELSC4.PRO - contains VELSCI (IDL procedure). Uses BETAT3.DAT. Faster for second and following calls. FRD and VLOS are scalar.

### 2.7.3 SOL Procedure

One of the IDL procedures was converted to the language SOL. The procedure is in the file VELSC1SOL.PRO and is effectively identical to the procedure in the IDL file VELSC1.PRO. All of the input and output parameters, etc., are identical.

## CHAPTER 3

### ANALYSIS OF UVSP DOPPLERGRAMS AND MAGNETOGRAMS AND THEIR CALIBRATION USING THE ORBITAL VELOCITY OF THE SMM SPACECRAFT

#### 3.1 INTRODUCTION

The provision in the Ultraviolet Spectrometer and Polarimeter (UVSP) experiment (Woodgate et al. 1980) on the Solar Maximum Mission (SMM) spacecraft of pairs of exit slits allowed different parts of one emission line (red and blue wings) to be observed simultaneously. Comparison of the intensities in the two parts of the line made it possible to observe relatively rapidly the line-of-sight components of the velocity (the dopplergram observing mode) and, when the polarimeter was also being used to measure the circular polarization caused by the Zeeman effect, the magnetic field (the magnetogram mode). The magnetogram mode also produced the same velocity information as the dopplergram mode. A procedure for analyzing dopplergrams and magnetograms obtained with wide exit slits has been described by Henze et al. (1982).

To convert the observed dopplergram and magnetogram signals to line-of-sight components of the velocity and magnetic field, one must know the width of the emission line for each pixel. (We assume a gaussian line profile where the width is specified by the doppler width. We also assume that there is no continuum emission.) A line-width calibration feature was included in the control system for the instrument. This feature, which was not always activated during the period of SMM operations in 1980, allowed periodic shifts by a known amount of the spectrometer grating and, therefore, of the line relative to the exit slits. The known shift thus provided an artificial velocity to calibrate the measured signal. A method of analysis using this feature was also described by Henze et al. (1982). When the feature was not used, it is still possible under certain conditions to determine the line width using the line-of-sight component of the orbital velocity of the spacecraft as the calibration reference. The primary purpose of this paper is to describe this method which uses the technique of least squares to fit the observed doppler shift signal for a pixel to the known line-of-sight component of the spacecraft velocity. The fitting procedure yields the doppler width and the offset for the pixel of the mean

position of the line relative to the position of the exit slits. The method is feasible because the maximum doppler shift due to the spacecraft motion is a significant fraction of the typical solar line widths.

There are several necessary conditions for application of the method. The observational data should consist of many repetitions of the dopplergram or magnetogram raster with the total duration covering a large fraction of the spacecraft orbit so that the line-of-sight component of the spacecraft velocity varied significantly during the observing sequence. There should have been no large secular or long-duration changes in the velocity of the solar emitting region during the observing sequence. Finally, the line width must have been constant during the observing sequence.

As background for the description of the calibration method and to show where the doppler width is required, we also summarize the theoretical expressions for conversion of the observed signals to velocities and magnetic fields. Although, as mentioned above, the expressions for wide exit slits have been published previously, those for narrow exit slits have not.

### 3.2 THEORETICAL INTERPRETATION OF DOPPLERGRAM AND MAGNETOGRAM SIGNALS

There are two types of exit slits used for dopplergrams and magnetograms in the UVSP: wide and narrow slits. Each member of a wide pair is  $0.3 \text{ \AA}$  wide in second order; the two members are exactly adjacent so that the entire line is effectively covered by the pair of slits. Each member of a narrow pair is  $0.03 \text{ \AA}$  wide in second order; the centers of the two members are  $0.294 \text{ \AA}$  apart at a wavelength of  $1548 \text{ \AA}$  (Athay et al. 1982). An illustration of the position of the wide and narrow exit slits relative to line profiles with two different widths is given in Figure 1 of the paper by Gurman and Athay (1983). In the remainder of this paper, the wide slits will be assumed to be semi-infinitely wide (so that together, the pair always cover the entire line) and the narrow slits assumed to be infinitesimally wide.

In the UVSP dopplergram or magnetogram observation, the observed doppler shift signal is defined as

$$R_V \equiv \frac{I_r - I_b}{I_r + I_b}, \quad (1)$$

where  $I$  is the intensity (integrated across the exit slit) and  $r$  and  $b$  denote the exit slits for the red and blue wings of the line. In a UVSP magnetogram observation, the observed magnetic circular polarization signal is defined as

$$R_m \equiv \frac{1}{2} \left( \frac{V_r}{I_r} - \frac{V_b}{I_b} \right), \quad (2)$$

where  $V$  is the Stokes parameter for circular polarization.

The line-of-sight velocity  $v$  is related to the line shift  $\Delta\lambda_V$  by

$$v = (c/\lambda_0)\Delta\lambda_V. \quad (3)$$

In addition to this doppler shift, any offset due to the non-ideal positioning of the line relative to the pair of exit slits will add a constant offset term to the line shift and thus to the velocity. For wide slits (Tandberg-Hanssen et al. 1981),

$$\Delta\lambda_V = \Delta\lambda_D \operatorname{inverf}(R_V), \quad (4)$$

where  $\Delta\lambda_D$  is the doppler width and  $\operatorname{inverf}$  is the inverse error function. If the shift is small ( $\Delta\lambda_V/\Delta\lambda_D \ll 1$ ),

$$\Delta\lambda_V \approx \Delta\lambda_D (\pi^{1/2}/2) R_V. \quad (5)$$

For narrow slits,

$$\Delta\lambda_V = (\Delta\lambda_D^2/\Delta\lambda_{\text{sep}}) \operatorname{arctanh}(R_V), \quad (6)$$

where  $\Delta\lambda_{\text{sep}}$  is the wavelength separation between the two exit slits and  $\operatorname{arctanh}$  is the inverse hyperbolic tangent function. If the shift is small,

$$\Delta\lambda_V \approx (\Delta\lambda_D^2/\Delta\lambda_{\text{sep}}) R_V. \quad (7)$$



The magnetic field  $B$  is related to the Zeeman splitting  $\Delta\lambda_B$  by

$$B = \frac{4\pi m c^2}{e\lambda^2 g_{\text{eff}}} \Delta\lambda_B . \quad (8)$$

For wide slits (Henze et al. 1982),

$$\Delta\lambda_B \cos\gamma = \Delta\lambda_D(\pi^{1/2}/2) R_m \left\{ [1 - \text{erf}^2(\Delta\lambda_V/\Delta\lambda_D)] \exp(\Delta\lambda_V/\Delta\lambda_D)^2 \right\} , \quad (9)$$

where  $\gamma$  is the angle between the field and the line of sight. If the line shift is small,

$$\Delta\lambda_B \cos\gamma \approx \Delta\lambda_D(\pi^{1/2}/2) R_m . \quad (10)$$

For narrow slits,

$$\Delta\lambda_B \cos\gamma = (\Delta\lambda_D^2/\Delta\lambda_{\text{sep}}) R_m , \quad (11)$$

which is independent of the line shift.

### 3.3 CALIBRATION USING SPACECRAFT ORBITAL MOTION

The basic method consists of fitting the appropriate function (inverf or arctanh) of the observed values of the doppler shift signal  $R_V$  for a pixel to a linear function of  $v_{SC}$ , the time-varying component of the spacecraft orbital velocity along the line of sight from the spacecraft to the sun. The spacecraft velocity component is calculated from the orbital ephemeris for the time of each observation as explained in Chapter 2 of this report. Maximum values are approximately  $\pm 7.5 \text{ km s}^{-1}$ .

For wide slits,

$$\text{inverf}(R_V) = a_0 + a_1 v_{SC} \quad (12)$$

For narrow slits,

$$\text{arctanh}(R_V) = a_0 + a_1 v_{SC} . \quad (13)$$

The least squares fitting procedure yields the parameters  $a_0$  and  $a_1$ ; their uncertainties are proportional to the standard deviation of the difference between the observed function of  $R_V$  and the fitted curve (Bevington 1969). Then, for wide slits,

$$\Delta\lambda_D = \lambda_0/(ca_1) , \quad (14)$$

and, for narrow slits,

$$\Delta\lambda_D = [(\lambda_0\Delta\lambda_{sep})/ca_1]^{1/2} . \quad (15)$$

For both types of slits,

$$v_{off} = a_0/a_1 , \quad (16)$$

where the offset velocity  $v_{off}$  includes both any steady line-of-sight velocity on the sun and the component due to the possible non-ideal position of the exit slits relative to the line. The uncertainties for the doppler width and the offset velocity can be obtained by propagating the uncertainties for  $a_0$  and  $a_1$  through Equations 14 to 16.

The method described above has been incorporated in an IDL procedure for convenient calculation on a computer.

### 3.4 APPLICATION TO WIDE-SLIT MAGNETOGRAMS

As a demonstration of the method, it has been applied to two magnetogram observations analyzed previously by Henze et al. (1982). The data were obtained in the C IV line at 1548 Å in the umbra of a sunspot on 23 and 25 October 1980; the exact locations are shown in Figure 1 of the paper by Henze et al.

Figure 3-1 shows the fit for one pixel in one of the magnetograms (UVSP Experiment 14398) of the observed doppler shift signal (converted to velocity) to the line-of-sight component of the spacecraft velocity. The complete sequence displayed here consisted of 256 repetitions of 5.056 s each. The observed curve shows fluctuations due to statistical noise (high frequency, small amplitude) and umbral oscillations (~150 s period, ~3 km s<sup>-1</sup> amplitude). Although both sources of fluctuations

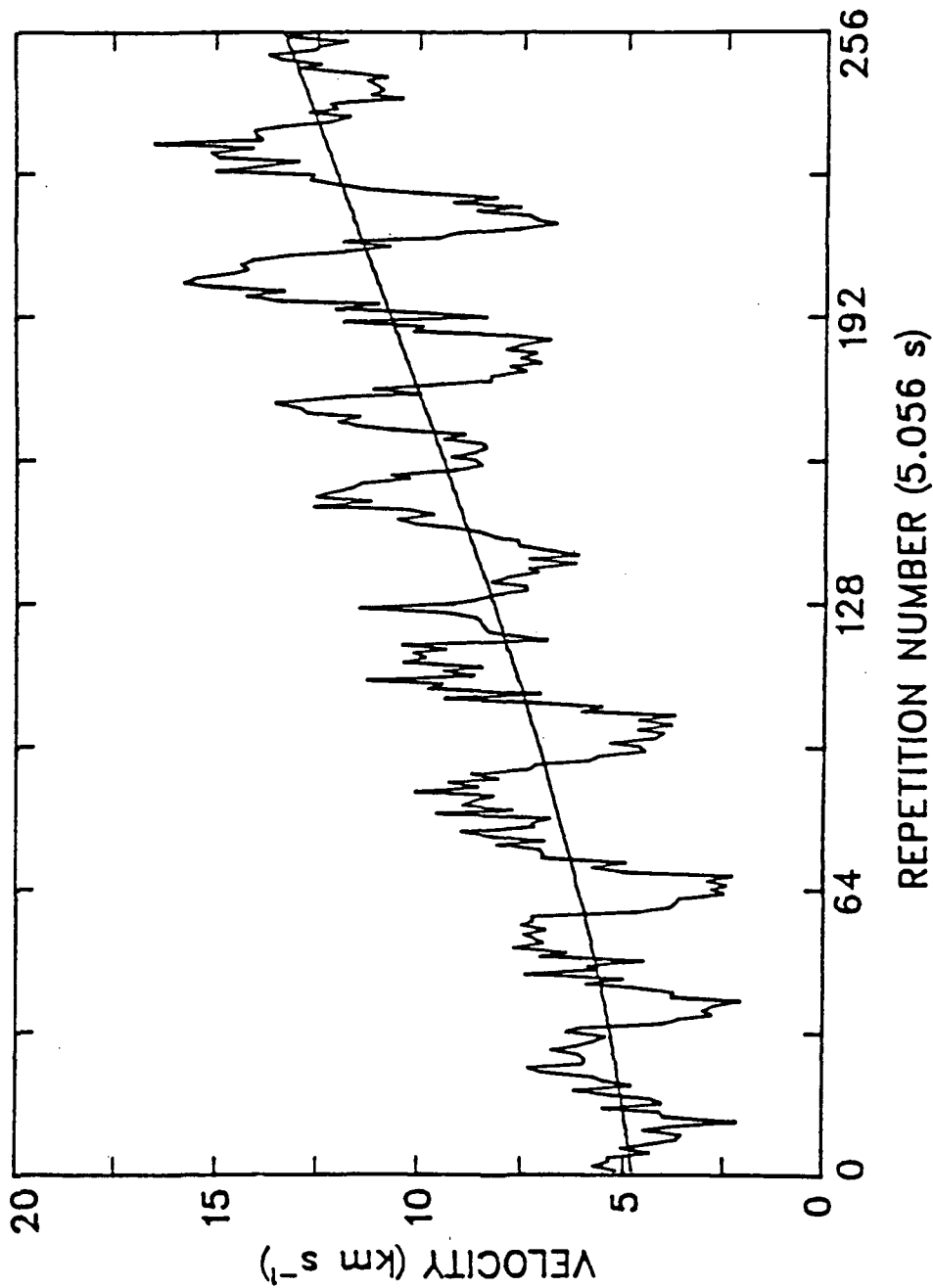


Figure 3-1. Example illustrating the method described in this paper. Data are for Pixel 5 in UVSP Experiment 14398 obtained 25 October 1980, 00:33 - 00:54 UT. The irregular curve is the observed doppler shift signal converted to velocity using the doppler width determined by the method. The smooth curve is the line-of-sight component of the orbital motion of the spacecraft shifted vertically by an amount also determined by the method. The vertical offset includes both any steady or flow velocity on the sun and the deviation of the exit slits from the true or absolute position of line center of zero velocity.

contribute to the formal uncertainties in the resulting parameters, the good fit of the general trend of the observed curve to the spacecraft curve and the large number of measurements causes those uncertainties to be small.

The numerical results for all five pixels are given in Table I. The doppler widths and the offset velocities along with their uncertainties (1 sigma) were obtained as described above. The offset velocities are all large and of the same sign, indicating that the exit slits were not well centered on the line. The measured values of the doppler width were then used to infer improved values of the magnetic field from the observed circular polarization signals; previously, the widths had been assumed to be 100 mÅ for all of the pixels. Because the values of the inferred fields are not greatly changed, the conclusions of Henze et al. (1982) about the existence of fields of the order of 1000 gauss in the transition region above a sunspot are not affected.

Table I also compares two different approaches to determining the magnetic field. In one approach, the full expression in Equation 9 was used for calculating the Zeeman splitting, and the magnetic field was determined separately for each repetition. The mean value is given in Table I where the uncertainty is the standard deviation of the mean. Using the other approach, Henze et al. (1982) summed the observed count rates over all 256 repetitions at each pixel and waveplate position before performing the magnetic field analyses; they also used the approximation in Equation 10. The uncertainty was derived from the statistical uncertainty in the count rates. Their results are also given in Table I after correction for the doppler width obtained here. The two methods yield similar values for the magnetic fields which agree well within the uncertainties. However, it should be better in principle to use the first approach, determining the magnetic field separately for each repetition and then taking the mean. The uncertainties also agree closely, thus indicating that the main source of random error in the magnetic field determination in this data set is the statistical counting noise and not any real intensity or magnetic field fluctuations on the sun. Of course, in other observations where the count rates are higher and the statistical noise in the results lower, real fluctuations may contribute significantly to the uncertainties.

TABLE I

Offset Velocity, Doppler Width, and Longitudinal  
Magnetic Field, UVSP Experiment 14398

Pixel	$v_{\text{off}}$ ( $\text{km s}^{-1}$ )	$\Delta\lambda_D$ ( $\text{m}\text{\AA}$ )	$B \cos \gamma^*$ (gauss)	$B \cos \gamma^{**}$ (gauss)
1	$16.4 \pm 0.7$	$94 \pm 4$	$-1320 \pm 630$	$-1090 \pm 620$
2	$14.4 \pm 0.6$	$88 \pm 4$	$-320 \pm 500$	$-370 \pm 480$
3	$10.1 \pm 0.5$	$80 \pm 3$	$-1010 \pm 430$	$-830 \pm 360$
4	$10.6 \pm 0.5$	$84 \pm 3$	$-960 \pm 330$	$-940 \pm 290$
5	$11.8 \pm 0.6$	$89 \pm 4$	$-1060 \pm 320$	$-1010 \pm 300$

\* Mean of results using Equation 9 for each repetition.

\*\* From Henze *et al.* (1982) but corrected for doppler width given here instead of the previously assumed value of 100  $\text{m}\text{\AA}$ .

As a check on the method, it was also applied to a calibrated magnetogram (UVSP Experiment 14302). The sequence contained 135 repetitions of 15.5 s each. Table II compares the results for those pixels that showed no systematic changes during the observations except for periodic oscillations. The widths obtained by Henze et al. (1982) were from the analysis of the first occurrence of the special calibration shift in the sequence (the 16th repetition). The results agree well. The small uncertainties in the results from this paper are due to the inclusion of many more repetitions in the analysis.

TABLE II  
Comparison of Methods of Calibration of the Line Width,  
UVSP Experiment 14302

Pixel	$\Delta\lambda_D$ (mÅ)		Pixel	$\Delta\lambda_D$ (mÅ)		Pixel	$\Delta\lambda_D$ (mÅ)	
	*	**		*	**		*	**
1	144 ± 3	135	8	134 ± 2	139	15	136 ± 2	122
2	142 ± 2	137	9	152 ± 2	150	16	137 ± 1	126
3	109 ± 2	111	10	109 ± 1	100	17	112 ± 1	104
4	116 ± 3	124	11	101 ± 2	100	18	121 ± 1	117

\* From method described in this paper.

\*\* From Henze et al. (1982), based on special calibration feature.

### 3.5 COMPUTER PROCEDURES

Some of the calculations necessary to use the above method have been incorporated in procedures written in the languages IDL and SOL.

The procedures are in the files:

```
IDL - LSVCALIDL.PRO
SOL - LSVCALSQL.PRO.
```

Both files contain the procedure:

```
PRO LSVCAL,VSC,JSLIT,FRV,CV,DL,D,VOFF,SIGDL,D,SIGVOF,SIG.
```

Also needed are the procedures:

```
PRO INVERF, X, Y and
PRO ARCTNH, X, Y.
```

They are included in the SOL file named above and are automatically compiled when the IDL file is compiled. The IDL versions are in the files INVERF.PRO and ARCTNH.PRO. Comments included in the files explain all of the parameters.

### 3.6 CONCLUSIONS

A method of determining the doppler width for each pixel and thereby calibrating UVSP dopplergrams and magnetograms using the line-of-sight component of the spacecraft orbital velocity has been described and illustrated. The method is useful when the special UVSP calibration feature was not activated, as was often the case during the period of SMM operations in 1980. The method requires the assumptions of constant doppler width and constant mean doppler shift (i.e., line-of-sight component of the flow velocity) during the observing sequence. The sequence must be long enough to determine the parameters to the desired degree of accuracy. If there are any oscillations present, then the duration should include several complete periods. Because of these restrictions, a better approach in the event that future SMM/UVSP observations become possible would be to invoke the normal calibration shift on every second raster, thus assuring an almost continuous calibration for the line widths. This procedure was used occasionally during 1980 and was called the Double Dopplergram Determination by Simon et al. (1982).

CHAPTER 4  
UVSP POLARIZATION ANALYSIS PROCEDURES

This chapter describes the analysis of UVSP polarization observations. Such observations are required, for example, to measure the longitudinal magnetic field as described in another chapter.

4.1 POLARIZATION SIGNAL

For a polarized light source described by the Stokes parameters, I, Q, U, V (also sometimes denoted by  $S_0, S_1, S_2, S_3$ ), the rotating waveplate in the UVSP modulates the detected signal  $\Phi$  as a function of the angle  $\omega$  of the waveplate fast axis:

$$\begin{aligned} \Phi(\omega) = K[ & I + p(a \cos 2\theta + b \sin 2\theta \sin 4\omega + b \cos 2\theta \cos 4\omega)Q + \\ & + p(-a \sin 2\theta - b \cos 2\theta \sin 4\omega + b \sin 2\theta \cos 4\omega)U + \\ & + p \sin \delta (\cos 2\theta \sin 2\omega - \sin 2\theta \cos 2\omega)V ], \end{aligned} \quad (1)$$

where K is the instrumental efficiency for the detector (including detector sensitivity, mirror and grating reflectivities, telescope collecting area, entrance slit solid angle, integration time, and waveplate transmissivity), p the degree of polarization of the analyzer (grating in this case),  $\theta$  the angle of analyzer axis,  $\delta$  the retardance of the waveplate,  $a = (1 + \cos \delta)/2$ , and  $b = (1 - \cos \delta)/2$ . The angles  $\omega$  and  $\theta$  are both positive clockwise (the direction of the waveplate rotation) when looking toward the light source and are measured relative to the same arbitrary reference direction, chosen to be the positive UVSP X axis in the instrument so that  $\theta = 0$ . In the usual spacecraft roll orientation, the positive X axis pointed to solar north. At the wavelength of 1548 Å,  $p = -0.65$  and  $\delta = 270^\circ$ . The waveplate position at which the first data point is measured in any UVSP polarization observation is at  $\omega = 315^\circ$ . Equation (1) is a Fourier series and the observed values of  $\Phi(\omega)$  can be Fourier analyzed to determine the coefficients and thus the Stokes parameters.



## 4.2 MAGNETOGRAMS

In magnetogram observations, only four equally spaced measurements were made so that the  $4\omega$  components (and thus the linear Stokes parameters,  $Q$  and  $U$ , which are expected to be small with the wide exit slits, cannot be determined. Also, the constant ( $0\omega$ )  $paQ$  term is ignored because it is expected that  $Q \ll I$ . Equation (1) then simplifies to

$$\Phi(\omega) = K[I + p \sin\delta V \sin 2\omega] . \quad (2)$$

The Fourier analysis yields

$$KI = [\Phi(315^\circ) + \Phi(45^\circ) + \Phi(135^\circ) + \Phi(225^\circ)]/4 \quad (3)$$

and

$$KV = -[\Phi(315^\circ) - \Phi(45^\circ) + \Phi(135^\circ) - \Phi(225^\circ)]/(4p \sin\delta) . \quad (4)$$

The fractional circular polarization is then  $V/I$ .

## 4.3 POLARGRAMS

Although UVSP polargrams can be made with any number of waveplate positions, the most common experiment definition would have sixteen equally spaced measurements (i.e.,  $22.5^\circ$  apart). For  $\theta = 0$ , Equation (1) becomes

$$\begin{aligned} \Phi(\omega) = K[I + paQ + p \sin\delta V \sin 2\omega \\ + pbQ \cos 4\omega - pbU \sin 4\omega] . \end{aligned} \quad (5)$$

To make the following equations easier to understand, let us denote the measurements at different waveplate positions as follows:

$$\Phi_1 = \Phi(315^\circ), \quad \Phi_2 = \Phi(337.5^\circ),$$

$$\Phi_3 = \Phi(0^\circ), \quad \Phi_4 = \Phi(22.5^\circ),$$

$$\Phi_5 = \Phi(45^\circ), \quad \Phi_6 = \Phi(67.5^\circ),$$

$$\Phi_7 = \Phi(90^\circ), \quad \Phi_8 = \Phi(112.5^\circ),$$

$$\Phi_9 = \Phi(135^\circ), \quad \Phi_{10} = \Phi(157.5^\circ),$$

$$\Phi_{11} = \Phi(180^\circ), \quad \Phi_{12} = \Phi(202.5^\circ),$$

$$\Phi_{13} = \Phi(225^\circ), \quad \Phi_{14} = \Phi(247.5^\circ),$$

$$\Phi_{15} = \Phi(270^\circ), \quad \Phi_{16} = \Phi(292.5^\circ).$$

The Fourier analysis yields

$$KI = \frac{1}{16} \sum_{i=1}^{16} \Phi_i + a[\Phi_1 - \Phi_3 + \Phi_5 - \Phi_7 + \Phi_9 - \Phi_{11} + \Phi_{13} - \Phi_{15}]/(8b), \quad (6)$$

which, if the polarization is small, simplifies to

$$KI \approx \frac{1}{16} \sum_{i=1}^{16} \Phi_i. \quad (7)$$

The Fourier analysis also yields

$$KQ = [\Phi_1 - \Phi_3 + \Phi_5 - \Phi_7 + \Phi_9 - \Phi_{11} + \Phi_{13} - \Phi_{15}]/(8pb), \quad (8)$$

$$KU = [\Phi_2 - \Phi_4 + \Phi_6 - \Phi_8 + \Phi_{10} - \Phi_{12} + \Phi_{14} - \Phi_{16}]/(8pb), \quad (9)$$

and

$$KV = - \left\{ [\Phi_1 - \Phi_5 + \Phi_9 - \Phi_{13}] + [\Phi_2 - \Phi_4 - \Phi_6 + \Phi_8 + \Phi_{10} - \Phi_{12} - \Phi_{14} + \Phi_{16}]/2^{\frac{1}{2}} \right\} / 8p \sin \delta. \quad (10)$$

The fractional linear polarization is then

$$P = (Q^2 + U^2)^{\frac{1}{2}}/I \quad (11)$$

and the angle  $\Psi$  of the linearly polarized component relative to the UVSP X-axis is given by

$$\tan 2\Psi = U/Q. \quad (12)$$

CHAPTER 5  
STATISTICAL UNCERTAINTIES

This chapter gives expressions for the statistical uncertainties in UVSP measurements of various quantities. The quantities themselves were mostly defined earlier in Chapter 3. The only uncertainty considered is that due to the fluctuations inherent in measuring a number of events such as photons counted by a detector.

5.1 BACKGROUND

The basis for the determination of an uncertainty is that the uncertainty  $\epsilon$  in the measurement of a number of counts  $\Phi$  is given by

$$\epsilon(\Phi) = \Phi^{\frac{1}{2}} . \quad (1)$$

The uncertainty used here is, therefore, the standard deviation (also often referred to as one sigma).

The uncertainty in the sum or difference of two quantities whose uncertainties or errors are independent is given by

$$\epsilon(A + B) = [\epsilon^2(A) + \epsilon^2(B)]^{\frac{1}{2}} \quad (2)$$

and

$$\epsilon(A - B) = [\epsilon^2(A) + \epsilon^2(B)]^{\frac{1}{2}} . \quad (3)$$

The uncertainty in the sum or difference of two quantities whose uncertainties or errors are not independent is given by

$$\epsilon(A + B) = \epsilon(A) + \epsilon(B) \quad (4)$$

and

$$\epsilon(A - B) = \epsilon(A) + \epsilon(B) . \quad (5)$$

Similar expressions are valid for the relative uncertainties of products and quotients. For independent uncertainties,

$$\epsilon(AB) = |AB| \left[ \frac{\epsilon^2(A)}{A^2} + \frac{\epsilon^2(B)}{B^2} \right]^{\frac{1}{2}} \quad (6)$$

and

$$\epsilon(A/B) = \left| \frac{A}{B} \right| \left[ \frac{\epsilon^2(A)}{A^2} + \frac{\epsilon^2(B)}{B^2} \right]^{\frac{1}{2}} . \quad (7)$$

For uncertainties or errors that are not independent,

$$\epsilon(AB) = |AB| \left[ \frac{\epsilon(A)}{|A|} + \frac{\epsilon(B)}{|B|} \right] \quad (8)$$

and

$$\epsilon(A/B) = \left| \frac{A}{B} \right| \left[ \frac{\epsilon(A)}{|A|} - \frac{\epsilon(B)}{|B|} \right] . \quad (9)$$

A special case is

$$\epsilon(A^2) = 2|A|\epsilon(A) ; \quad (10)$$

the inverse is

$$\epsilon(A^{\frac{1}{2}}) = \frac{\epsilon(A)}{2A^{\frac{1}{2}}} . \quad (11)$$

If a quantity is multiplied by a constant a, the uncertainty is

$$\epsilon(aA) = a \epsilon(A) . \quad (12)$$

## 5.2 POLARIZATION

The uncertainty in the intensity Stokes parameter depends on how many waveplate positions were used in the measurement. (Polarization effects are assumed to be small.) If N is the number of waveplate positions,

$$\epsilon(KI) = \frac{1}{N^{\frac{1}{2}}} (KI)^{\frac{1}{2}} , \quad (13)$$

where

N = 1 for dopplergrams,

N = 4 for most magnetograms,

N = 16 for most polargrams.

If N = 4,

$$\epsilon(KV) = \epsilon(KI)/(p \sin\delta) . \quad (14)$$

If N = 16,

$$\epsilon(KV) = 2^{\frac{1}{2}} \epsilon(KI)/(p \sin\delta) , \quad (15)$$

$$\epsilon(KQ) = 2^{\frac{1}{2}} \epsilon(KI)/(pb) , \quad (16)$$

and

$$\epsilon(KU) = \epsilon(KQ) . \quad (17)$$

Also, 
$$\epsilon(K[Q^2 + U^2]^{\frac{1}{2}}) = \epsilon(KQ) , \quad (18)$$

and 
$$\epsilon(\Psi) = \frac{1}{2} \text{arc sin} \left\{ \frac{\epsilon(KQ)}{K[Q^2 + U^2]^{\frac{1}{2}}} \right\} . \quad (19)$$

If the linear polarization is small,

$$\epsilon(P) = \epsilon([Q^2 + U^2]^{\frac{1}{2}})/I = \epsilon(KQ)/(KI) . \quad (20)$$

### 5.3 LINE INTENSITIES

The combined line intensity  $I_L$  is the sum of the two intensities  $I_r$  and  $I_b$ :

$$I_L = I_r + I_b , \quad (21)$$

where  $r$  and  $b$  denote the detectors in the red and blue wings, respectively. (For wide exit slits, this is the true total line intensity.) Because we are actually measuring counts (e.g.,  $K_r I_r$  instead of  $I_r$ ), we define the weighted sum of the two count rates:

$$[K_r K_b]^{\frac{1}{2}} I_L = R^{-\frac{1}{2}} K_r I_r + R^{\frac{1}{2}} K_b I_b , \quad (22)$$

where

$$R \equiv K_r / K_b . \quad (23)$$

The uncertainty is then

$$\epsilon\left([K_r K_b]^{\frac{1}{2}} I_L\right) = [R^{-1} \epsilon^2(K_r I_r) + R \epsilon^2(K_b I_b)]^{\frac{1}{2}} . \quad (24)$$

### 5.4 MAGNETOMETRY

If the polarization is small,

$$\epsilon(V/I) = \epsilon(V)/I = \epsilon(KV)/(KI) . \quad (25)$$

The uncertainty in the observed magnetic circular polarization signal is

$$\epsilon(R_m) = \frac{1}{2} \left[ \frac{\epsilon^2(K_r V_r)}{(K_r I_r)^2} + \frac{\epsilon^2(K_b V_b)}{(K_b I_b)^2} \right]^{\frac{1}{2}} . \quad (26)$$

For  $N = 4$ ,

$$\epsilon(R_m) = \left[ \frac{1}{K_r I_r} + \frac{1}{K_b I_b} \right]^{\frac{1}{2}} / (4 p \sin \delta) . \quad (27)$$

For  $N = 16$ ,

$$\epsilon(R_m) = 2^{\frac{1}{2}} \left[ \frac{1}{K_r I_r} + \frac{1}{K_b I_b} \right]^{\frac{1}{2}} / (8 p \sin \delta) . \quad (28)$$

Allowing for any uncertainty in the doppler shift (such as that resulting from the least-squares fitting technique using the spacecraft velocity described in Chapter 3) and assuming that the doppler line shift is small, we obtain, for wide exit slits,

$$\epsilon(\Delta\lambda_B \cos\gamma) = |\Delta\lambda_B \cos\gamma| \left[ \frac{\epsilon^2(\Delta\lambda_D)}{\Delta\lambda_D^2} + \frac{\epsilon^2(R_m)}{R_m^2} \right]^{\frac{1}{2}} . \quad (29)$$

For narrow exit slits,

$$\epsilon(\Delta\lambda_B \cos\gamma) = |\Delta\lambda_B \cos\gamma| \left[ \frac{4\epsilon^2(\Delta\lambda_D)}{\Delta\lambda_D^2} + \frac{\epsilon^2(R_m)}{R_m^2} \right]^{\frac{1}{2}} . \quad (30)$$

For either type of exit slit,

$$\frac{\epsilon(B \cos\gamma)}{|B \cos\gamma|} = \frac{\epsilon(\Delta\lambda_B \cos\gamma)}{|\Delta\lambda_B \cos\gamma|} . \quad (31)$$

## 5.5 VELOCITY MEASUREMENTS

If the uncertainties in the numerator and denominator of the observed doppler shift signal are not assumed to be small and if the doppler shift itself not assumed to be small, the uncertainty in the shift signal is

$$\epsilon(R_V) = (1 + |R_V|) \frac{\epsilon([K_r K_b]^{\frac{1}{2}} I_L)}{[K_r K_b]^{\frac{1}{2}} I_L} . \quad (32)$$

Including the uncertainty in the doppler width yields, for wide exit slits,

$$\epsilon(\Delta\lambda_V) = |\Delta\lambda_V| \left[ \frac{\epsilon^2(\Delta\lambda_D)}{\Delta\lambda_D^2} + \frac{\epsilon^2(R_V)}{R_V^2} \right]^{\frac{1}{2}} . \quad (33)$$

For narrow exit slits,

$$\epsilon(\Delta\lambda_V) = |\Delta\lambda_V| \left[ \frac{4 \epsilon^2(\Delta\lambda_D)}{\Delta\lambda_D^2} + \frac{\epsilon^2(R_V)}{R_V^2} \right]^{\frac{1}{2}} \quad (34)$$

For either type of exit slit,

$$\frac{\epsilon(v)}{|v|} = \frac{\epsilon(\Delta\lambda_V)}{|\Delta\lambda_V|} \quad (35)$$

## REFERENCES

- Athay, R. G., Gurman, J. B., Henze, W., and Shine, R. A.: 1982, Astrophys. J. 261, 684.
- Bevington, P. R.: 1969, Data Reduction and Error Analysis for the Physical Sciences, McGraw-Hill Book Co., New York, pp. 99-115.
- Gurman, J. B., and Athay, R. G.: 1983, Astrophys. J. 273, 374.
- Henze, W.: 1979, Teledyne Brown Engineering Interim Contract Report PI79-MSFC-2323.
- Henze, W., Tandberg-Hanssen, E., Hagyard, M. J., Woodgate, B. E. Shine, R. A., Beckers, J. M., Bruner, M., Gurman, J. B., Hyder, C. L., and West, E. A.: 1982, Solar Phys. 81, 231.
- Simon, G., Mein, P., Vial, J. C., Shine, R. A., and Woodgate, B. E.: 1982, Astron. Astrophys. 115, 367.
- Tandberg-Hanssen, E., Athay, R. G., Beckers, J. M., Brandt, J. C., Bruner, E. C., Chapman, R. D., Cheng, C. C., Gurman, J. B., Henze, W., Hyder, C. L., Michalitsianos, A. G., Shine, R. A., and Woodgate, B. E.: 1981, Astrophys. J. Letters 244, L127.
- Woodgate, B. E., Tandberg-Hanssen, E. A., Bruner, E. C., Beckers, J. M., Brandt, J. C., Henze, W., Hyder, C. L., Kalet, M. W., Kenny, P. J., Knox, E. D., Michalitsianos, A. G., Rehse, R., Shine, R. A., and Tinsley, H. D.: 1980, Solar Phys. 65, 73.